Solar Energy Materials & Solar Cells 161 (2017) 157–161

Contents lists available at ScienceDirect

Solar Energy Materials & Solar Cells

journal homepage: www.elsevier.com/locate/solmat

Solution processed Cu_2CdSnS_4 as a low-cost inorganic hole transport material for polymer solar cells

M. Suresh Kumar[a,b], Kallol Mohanta[a], Sudip K. Batabyal[b,*]

[a] Hybrid Solar Energy Lab, Nanotech Research Innovation & Incubation Centre, PSG Institute of Advanced Studies, Coimbatore, Tamil Nadu 641004, India
[b] Amrita Centre for Industrial Research & Innovation (ACIRI), Amrita School of Engineering, Amrita Vishwa Vidyapeetham, Amrita University, Coimbatore, Tamil Nadu 641112, India

ARTICLE INFO

Keywords:
Organic photovoltaics
Inorganic hole transport layer
$CuCdSnS_4$
PEDOT:PSS replacement

ABSTRACT

The inefficient charge separation is one of the major impediments to improve the overall power conversion efficiency of the organic photovoltaics. Herein we demonstrate a new inorganic hole transporting materials for organic photovoltaics. Cu_2CdSnS_4 hole transport layer was deposited by solution based approach in low temperature by simple method. The thickness dependence of Cu_2CdSnS_4 hole transport layer on photovoltaic performance of organic solar cells was studied in details. The hole extraction activity of Cu_2CdSnS_4 thin films were compared with the reference PEDOT:PSS hole transport layer in the fabrication of P3HT:PCBM solar cells.

1. Introduction

Polymer solar cells (PSCs) have attracted tremendous research interest worldwide owing to their advantages such as solution-processability, light weight, easy fabrication, low-cost, and mechanical flexibility [1–6]. The performance of PSCs improves with the bulk heterojunction formations, in which the electron donor (D) and acceptor (A) materials are blended together to form interpenetrating network between D-A for the adequate dissociation of excitons. Moreover, solution-processed bulk heterojunction (BHJ) solar cells deliver salient advantages includes, greater mechanical robustness, simple blending, and better power conversion efficiencies (PCEs) [7]. One of the most prominent and well researched photoactive absorber layer till date is a blend of poly (3-hexylthiophene) (P3HT) as an electron donor and [6,6]-phenyl-C_{61}-butyric acid methyl ester ($PC_{61}BM$) as an electron acceptor [8]. The basic organic solar cells (OSCs) comprise of device structure consisting of a photosensitive layer sandwiched between two metal electrodes, one of which is transparent for the light to pass through. The interfacial buffer layers between the electrodes and the active layer employs better transportation property. Once the excitons in the active layer gets dissociated, generated electrons and holes have to be properly transported to their respective electrodes through the buffer layer. The poly(3,4-ethylenedioxythiophene): polystyrenesulfonate (PEDOT:PSS) is traditionally used for anode interfacial buffer layer in the conventional PSCs due to its pertinent advantages such as ease in processability, smooth surface topography, and matching work function with HOMO of many donor-type organic semiconductors [9]. However, the acidic and hygroscopic nature of PEDOT:PSS makes the indium tin oxide (ITO) surface vulnerable to degradation at elevated temperatures, inefficient electron-blocking performance, and thus negatively contribute to performance and stability of PSCs under ambient conditions [10,11]. Therefore, a range of alternative hole transport layer (HTL) materials have been investigated in an effort to address these issues. Hence, it was long overdue to find an alternative and suitable hole transport materials to replace PEDOT:PSS. Transition metal oxides, such as nickel oxide (NiO_x) [12], molybdenum oxide (MoO_3) [13], vanadium oxide (V_2O_5) [14] and tungsten oxide (WO_3) [15] have been extensively used as anode buffer layers. The photovoltaic devices from these HTLs have shown improved device parameters than that of PEDOT:PSS. However, the processability of these inorganic materials involves tricky and knotty methods. These inorganic materials are insoluble in many solvents and are usually deposited through vacuum techniques like thermal or electron beam evaporation, sputtering or pulsed-laser deposition. Substantially evaporation of the materials in high vacuum tools is more expensive and more complicated than solution-based approaches [16].

Since few decades, the stoichiometric Cu_2–II–IV–VI_4 (II=Zn, Cd, Hg; IV=Si, Ge, Sn; VI=S, Se, Te) chalcogenide semiconductors have shown potential applications in the field of photovoltaics [17,18] and thermoelectric devices [19–22]. Like CZTS, Cu_2CdSnS_4 (CCTS) possess large absorption coefficient, abundant availability and promising band gap. Thin-films of CZTS can be deposited by various approaches, such as sputtering [23], thermal evaporation [24], spray pyrolysis [25],

* Corresponding author.
E-mail addresses: batabyal@gmail.com, s_batabyal@cb.amrita.edu (S.K. Batabyal).

http://dx.doi.org/10.1016/j.solmat.2016.11.028
Received 31 August 2016; Received in revised form 4 November 2016; Accepted 23 November 2016
Available online 05 December 2016
0927-0248/

chemical bath deposition [26], spin coating [19] and so on. The solution based approaches are based one from hydrazine solution [27], the sol–gel sulfurizing method [28], electro deposition using ionic liquids [29], followed by annealing at a high-temperature. In this work, we demonstrate the capability of using solution-processed CCTS nanoparticles as a low cost inorganic p-type buffer layer between the anode and P3HT:PCBM blend. From the practical point of view, fabrication of CCTS layer also in line with the other layer of the polymeric solar cell i.e. based on low temperature solution processed method. The buffer layer thickness has been varied to assess how the nanostructural nature of the CCTS effect on the cells' performance. Along with crystal structures, morphologies, optical and photo response properties of the as-prepared CCTS thin films were investigated in details to explain and support our observations. This is possibly the first time CCTS has been evaluated as a hole transporting material in organic solar cells.

2. Experimental details

2.1. Materials and reagents

Copper nitrate hexahydrate ($Cu(NO_3)_2·6H_2O$, > 90%), Cadmium nitrate tetrahydrate ($Cd(NO_3)_2·4H_2O$, > 90%), Tin chloride dihydrate ($SnCl_2·2H_2O$, > 90%), Thiourea (CH_4N_2S, 90%), 2-methoxyethanol and 1,2-dichlorobenzene are all of analytical grade and purchased from Merck. The poly(3,4-ethylenedioxythiophene):polystyrene sulfonate (PEDOT:PSS), the electron donor material poly(3-hexylthiophene) (P3HT) and electron acceptor material [6,6]-phenyl C_{61}butyric acid methyl ester ($PC_{61}BM$) were purchased from Sigma Aldrich. All the chemicals and solvents were used as received without any further purification.

2.2. Fabrication of Cu_2CdSnS_4 precursor

The stock solutions were prepared in four different glass vials consisting of $Cu(NO_3)_2·6H_2O$ (0.20 M), $SnCl_2·2H_2O$ (0.15 M), $Cd(NO_3)_2·4H_2O$ (0.15 M), CH_4N_2S (0.45 M) respectively by dissolving in 2-methoxyethanol. Then in a beaker, $SnCl_2$ solution was added drop wise to the above 0.2 M copper nitrate solution under continuous stirring followed by addition of thiourea solution and cadmium nitrate solution at room temperature. The resultant solution was further stirred for 1 h to obtain a homogeneous, colourless and transparent precursor solution.

2.3. Device fabrication

The ITO coated glass substrate (20 Ω/□) was used as a substrate for the device fabrication. The schematic structure of the organic solar cell is shown in Fig. 1. The substrates were cleaned in an ultrasonic bath with DI water, acetone, methanol, and isopropanol to remove any dust or organic residues present on the surface of the substrate. The substrates were then blown dry using nitrogen and treated with ultraviolet ozone (UVO) for 30 min to increase the wettabilty of the surface. P3HT (electron donor material) and $PC_{61}BM$ (electron acceptor material) were weighed (1:0.8 w/w) and dissolved in 1,2-dichlorobenzene (DCB) in a nitrogen-filled glove box. The solution was stirred at 45 °C for 15 h. The PEDOT:PSS solution was spin-coated at 3000 rpm for 60 s on the cleaned ITO substrates, followed by baking at 120 °C for 20 min on a hot plate. A reference cell was fabricated with PEDOT:PSS as hole transport layer. The CCTS solution was spin coated on cleaned ITO substrates at 2500 rpm for 45 s, followed by baking on a hot plate at 250 °C for 10 min in ambient condition. The thickness of the CCTS thin films were increased by repeated spin coating and annealing cycle. Sample A, Sample B, Sample C and Sample D were named which corresponds to the single layer CCTS, double layer CCTS, triple layer CCTS and quadruple layer CCTS respectively. P3HT:$PC_{61}BM$ was spin-coated at 1000 rpm for 60 s inside the glove box. Finally, the top metal electrode was formed through sequential deposition of LiF (6 nm) and Al cathode (120 nm) was deposited using thermal evaporator under vacuum (pressure: $5{\times}10^{-6}$ mbar). A shadow mask was used during thermal evaporation to define an active area of 0.5 cm^2. The completed device was post annealed at 120 °C for 30 min inside a vacuum chamber.

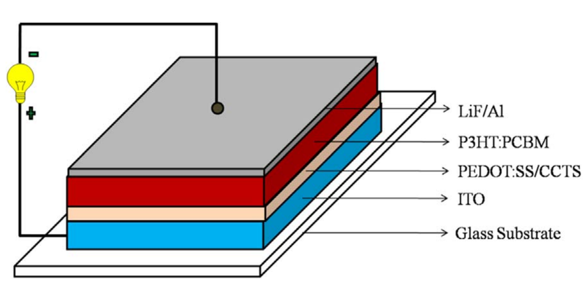

Fig. 1. : Schematic Structure of the Organic Solar Cell.

2.4. Characterizations

The surface topography of CCTS thin films were investigated by atomic force microscopy (AFM) measurements with a NT-MDT (Russia) in the tapping (semi-contact) mode. X-ray diffraction (XRD) patterns were recorded by PANalytical (Netherlands) with CuKα radiation of 0.154 nm. The morphology of Cu_2CdSnS_4 nanoparticles were analyzed by high resolution transmission electron microscopy (HRTEM) with JEOL 2100, Japan. The UV-Vis spectroscopy of CCTS thin film was investigated with a Shimadzu UV-1800 (Japan) Spectrometer. The current density-voltage (J-V) curves of organic solar cells were measured using a Keithley 2450 source measure unit under simulated 100 mW /cm^2 illumination (AM 1.5 G) in air.

3. Results and discussion

Spin coated CCTS film exhibits very weak X-ray diffraction peak because of less thickness. To understand the structural characteristics of the deposited sample we deposited a thick film by drop-casting the precursor solution on glass substrate. Fig. 2 illustrates the XRD pattern of the drop casted films over glass substrate. The diffraction peaks in XRD patterns can be indexed as those of cernyite structure of Cu_2CdSnS_4 where the peaks at 2θ=28.1°, 32.5°, 46.6°, 55.3°, 75.2° corresponds to the diffraction planes of (112), (200), (220), (312) and (332) orientation respectively, according to JCPDS 29–0537. The calculated diameter (D) of CCTS particles from the full width at half maximum (FWHM) of the strongest diffraction peak of the (112) plane

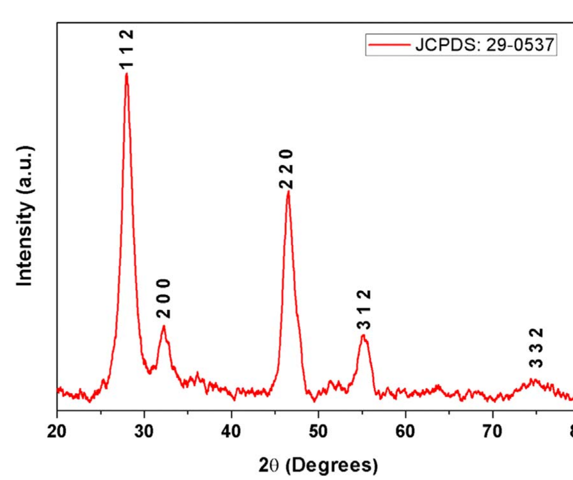

Fig. 2. : XRD patterns of Cu_2CdSnS_4 thin films.

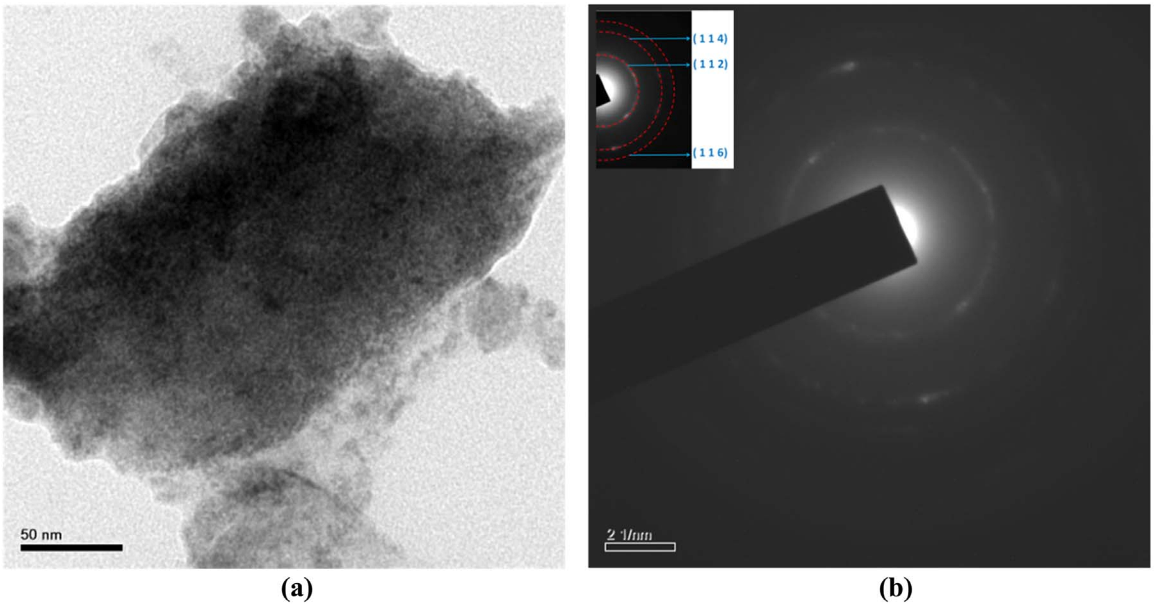

Fig. 3. HRTEM images of Cu_2CdSnS_4 nanoparticles (a) Morphology, (b) SAED pattern.

was about ca. 8.52 nm by Debye–Scherrer formula [30],

$$D = K\lambda(\beta cos\theta)^{-1}$$

where, K is a constant (0.9), λ is the wavelength of the X-ray source, β is the full width half maximum (FWHM) of (112) peak and θ is the Bragg angle of the (112) peak.

Fig. 3a illustrates the HRTEM image of CCTS particle collected from the as deposited thin film. The size of the nanoparticles were evaluated using Image-J software and were about 7–12 nm, which is consistent with the value calculated from the XRD pattern. Fig. 3b demonstrates the selective area diffraction pattern (SAED) of the individual nanocrystal obtained from TEM analysis, showing the nanocrystalline nature of the CCTS nanoparticles. Moreover, the diffraction spot corresponds to the *hkl* planes (112), (114) and (116) confirm the particles are of tetragonal structure (JCPDS 29-0537).

Fig. 4 shows the UV–Vis absorption spectra of the as deposited CCTS thin films. From the absorption spectra, no distinct peaks were observed where as a small hump was noticed at wavelength of around 380 nm. This hump shifts right to the higher wavelength with increase in thickness. As known, CCTS is a direct band gap semiconductor [30], so the band gap value can be estimated from the absorption spectra according to the following equation [31].

$$(\alpha h\nu)^2 = A(h\nu - E_g)$$

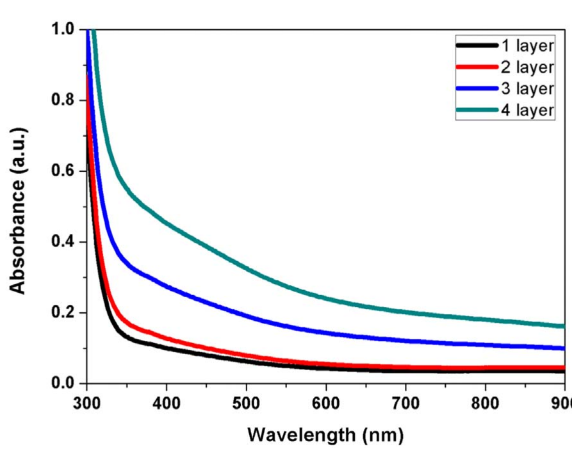

Fig. 4. Optical absorption spectra of Cu_2CdSnS_4 thin films of different thicknesses.

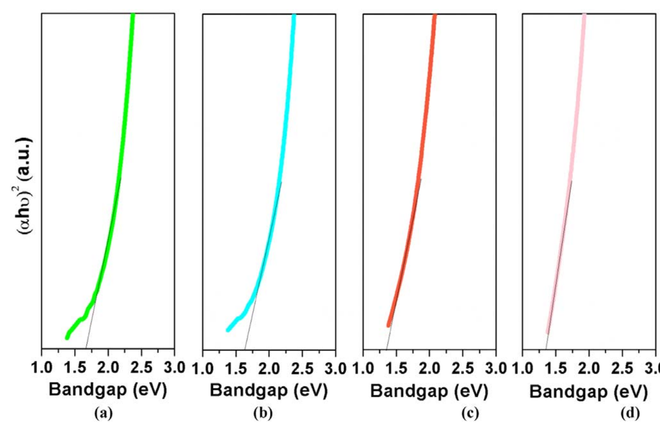

Fig. 5. Tauc plot for the band gap calculation (a) Band gap for 1 layer Cu_2CdSnS_4 thin film=1.65 eV, (b) Bandgap for 2 layers Cu_2CdSnS_4=1.60 eV, (c) Bandgap for 3 layers Cu_2CdSnS_4=1.35 eV, (d) Bandgap for 4 layers Cu_2CdSnS_4 =1.35 eV.

where, α is the absorption coefficient, A is a constant, E_g is the energy gap and hν is the incident photon energy. The optical band gap is deduced by extrapolating the linear portion of the $(\alpha h\nu)^2$ versus (hν) plot (Fig. 5**)** to meet the hν axis. The calculated band gap values for 1 layer, 2 layers, 3 layers and 4 layers CCTS thin films are 1.65 eV, 1.60 eV, 1.35 eV and 1.35 eV respectively. The band gap value of CCTS decreases with increase in the thickness as illustrated in Fig. 5. This confirms with increase in the thickness of the layers the particles get agglomerated and their size increases. From Fig. 4, it is also clear that the absorption spectrum of CCTS thin films covers the entire visible region which is optimum for the solar cell applications; also the absorption increases with the increase in thickness. Probably absorption of light in CCTS layer produces extra charge carriers which can contribute to light current of the solar cells [32]. So it is assumed that along with the hole transporting property, CCTS also has incremental contribution in photocurrent.

Atomic Force Microscope (AFM) images are used to analyze the surface topography and particle size distribution of the as deposited films. Fig. 6 manifests the 15×15 μm^2 tapping mode AFM images of as deposited CCTS thin films. The photovoltaic device performance significantly depends on the surface roughness of buffer layer. Greater surface roughness of a layers will hinder formation of an intimate contact with the active layer which results in reduced charge

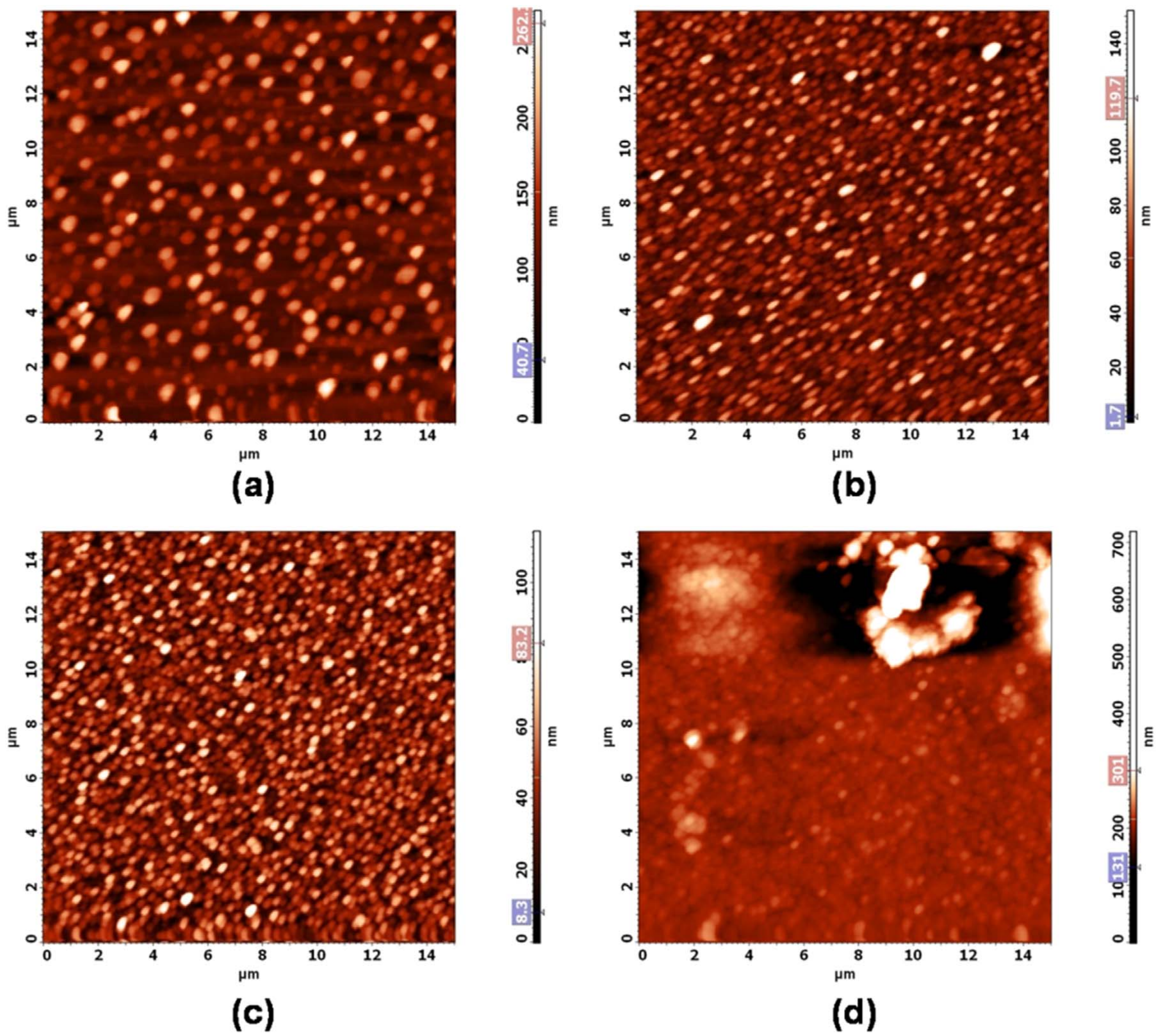

Fig. 6. AFM images of Cu_2CdSnS_4 thin film of different thicknesses (a) Layer 1 (L1), (b) Layer 2 (L2), (c) Layer 3 (L3), (d) Layer 4 (L4).

transport efficiency through the interface, and as a consequence, decreases the device performance. The average roughness (Sa) as calculated for the sample single layer of CCTS thin film (L1), 2 layers of CCTS thin film (L2), 3 layers of CCTS thin films (L3) and 4 layers of CCTS thin film (L4) were 23.54 nm, 13.11 nm, 11.07 nm and 21.00 nm respectively. L3 generate minimum surface roughness of 11.07 nm implying a more uniform coating over the surface when compared to L1, L2 and L4. Moreover, from Fig. 6, it was also clear that by increasing the number of layers, the compactness of the thin film was superior which may be due to filling of voids developed in the previous layer with additional layers. However, with increase in the layer thickness at one point, results in aggregation of the particles which may deter the transportation of the charge carriers and reduce the overall performance of the device. Thus, L3 was the optimum for the use of CCTS as hole transporting layer here.

Fig. 7 illustrates the current density–voltage (J–V) characteristics of the final organic photovoltaic devices under AM 1.5 G irradiance with intensity of 100 mW/cm^2. The short-circuit current density (Jsc), open-circuit voltage (Voc), maximum power (Pmax), fill factor (FF), and power conversion efficiency (PCE) of the OSCs with different CCTS HTL thickness and standard PEDOT:PSS HTL are summarized in Table 1. We notice that the PCE of the OSCs increases with increase in CCTS thickness and then decreases significantly. Further investigations reveal that no significant change in short circuit current density and open circuit voltage; however, there are some differences in the FF. The FF is mostly influenced by the nature of the films and their interfacial

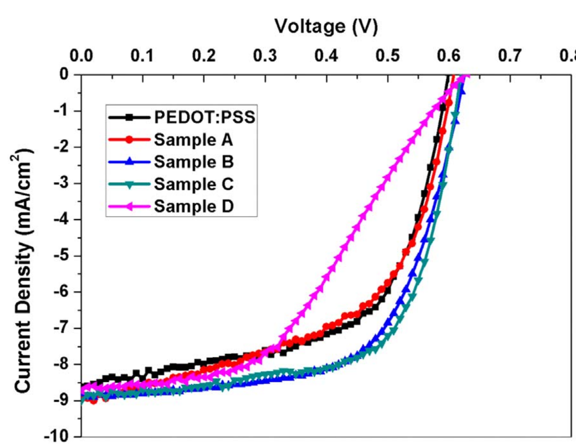

Fig. 7. : J–V characteristics of the OSCs under AM 1.5 G irradiance.

properties. According to Table 1 PCE of OSCs with CCTS HTL is comparable with standard PEDOT:PSS HTL. From the Table 1 it is also clear that PCE of sample C with 3 layers of CCTS having thickness of around 90 nm is higher compared to other samples. This increase in efficiency may be due to the uniform film thickness and compactness which generate optimum interface and improves the charge transfer dynamics. In our study, we have chosen Cu_2CdSnS_4 as a HTL material which has larger absorption coefficient of $> 10^4$ cm^{-1} and covers the

Table 1
Device parameters of organic solar cells under illumination with different thicknesses of Cu_2CdSnS_4 HTL compared with PEDOT:PSS HTL.

Device	Sample	HTL	Voc (V)	Jsc (mA/cm^2)	Pmax (mW)	FF (%)	PCE (%)
1	Reference cell	PEDOT:PSS	0.60	8.61	3.08	59.61	3.08
2	Sample A	CCTS	0.61	8.95	2.97	54.50	2.97
3	Sample B		0.62	8.80	3.51	64.29	3.51
4	Sample C		0.62	8.99	3.63	65.18	3.63
5	Sample D		0.62	8.71	2.41	44.54	2.41

entire visible region of the absorption spectra as shown in Fig. 4. The interface between the HTL and active layer would have produce extra exciton resulted in increase in photocurrent of the device. This nature of HTL material is also expected to be the reason for increase in the FF. As a conclusion, Cu_2CdSnS_4 HTL may be acts as both anode buffer layer and secondary active layer.

Generally metal chalcogenides are more stable in ambient condition than the organic materials. CCTS is the analogous compound of Cu_2ZnSnS_4 (CZTS) and $CuInGaS_2$ (CIGS). CIGS and CZTS are now widely used as photo absorber materials for thin film solar cell. In general manufacturer covers the warranty of the power output of these solar cells around 20–25 years [33]. Whereas the life span of OSCs are only few years [34]. Though the conclusions on stability of CCTS hole transporting layer need some further study with proper encapsulated device but we can predict the stability of the device with CCTS hole transporting layer will be much more than the PEDOT:PSS hole transporting layer.

4. Conclusions

In conclusion, we have successfully developed Cu_2CdSnS_4 thin films over ITO coated glass substrates and used as a hole transport material for the efficient transport of holes from the P3HT:PCBM blend to the ITO anode. The performance of the device with PEDOT:PSS HTL and Cu_2CdSnS_4 HTL has been compared. The effect of HTL morphology plays vital role in charge transport and the use of photosensitive HTLs assists with creation of additional excitons and contributes in improvement of overall power conversion efficiency of the organic solar cells.

Acknowledgement

S. K. Batabyal would like to thank the financial support from Amrita University start up grant (AMRITA/IFRP-01/2016-2017). K. Mohanta would like to acknowledge the support from Science and Engineering Research Board (SERB) of Department of Science and Technology (DST), GoI (SB/FTP/PS-167/2013) and Board of Research in Nuclear Science, Department of Atomic Energy, GoI (34/14/26/2014-BRNS/1749).

References

[1] W. Sun, H. Peng, Y. Li, W. Yan, Z. Liu, Z. Bian, et al., Solution-processed copper iodide as an inexpensive and effective anode buffer layer for polymer solar cells, J. Phys. Chem. C 118 (2014) 16806–16812.

[2] G. Yu, J. Gao, J. Hummelen, F. Wudl, A. Heeger, Polymer photovoltaic cells: enhanced efficiencies via a network of internal donor-acceptor heterojunctions, Science 270 (1995) 1789–1790.

[3] M. Kaltenbrunner, M.S. White, E.D. Glowacki, T. Sekitani, T. Someya, N.S. Sariciftci, S. Bauer, Ultrathin and lightweight organic solar cells with high flexibility, Nat. Commun. 3 (2012) 770.

[4] G. Li, R. Zhu, Y. Yang, Polymer solar cells, Nat. Photonics 6 (2012) 153–161.

[5] G. Dennler, M.C. Scharber, C.J. Brabec, Polymer-Fullerene bulk-heterojunction solar cells, Adv. Mater. 21 (2009) 1323–1338.

[6] C.J. Brabec, S. Gowrisanker, J.J.M. Halls, D. Laird, S. Jia, S.P. Williams, Polymer-fullerene bulk-heterojunction solar cells, Adv. Mater. 22 (2010) 3839–3856.

[7] K. Moorthy, S. Raman, R. Mohanraman, C. Chu, Solution-processable bismuth iodide nanosheets as hole transport layers for organic solar cells, Sol. Energy Mater. Sol. Cells 121 (2014) 35–41.

[8] M.T. Dang, L. Hirsch, G. Wantz, P3HT:PCBM, best seller in polymer photovoltaic research, Adv. Mater. 23 (2011) 3597–3602.

[9] M.P. de Jong, L.J. van Ijzendoorn, M.J.A. de Voigt, Stability of the interface between indium-tin-oxide and poly(3,4-ethylenedioxythiophene)/poly(styrenesulfonate) in polymer light-emitting diodes, Appl. Phys. Lett. 77 (2000) 2255.

[10] M. Jorgensen, K. Normann, F.C. Krebs, Stability/degradation of polymer solar cells, Sol. Energy Mater. Sol. Cells 92 (2008) 686–714.

[11] M.P. De Jong, L.J. Van IJzendoorn, M.J.A. De Voigt, Stability of the interface between indium-tin-oxide and poly(3,4-ethylenedioxythiophene)/poly (styrene-sulfonate) in polymer light-emitting diodes, Appl. Phys. Lett. 77 (2000) 2255–2257.

[12] M.D. Irwin, D.B. Buchholz, A.W. Hains, R.P.H. Chang, T.J. Marks, P-Type semiconducting nickel oxide as an efficiency-enhancing anode interfacial layer in polymer bulk-heterojunction solar cells, Proc. Natl. Acad. Sci. USA 105 (2008) 2783–2787.

[13] S. Murase, Y. Yang, Solution processed MoO3 interfacial layer for organic photovoltaics prepared by a facile synthesis method, Adv. Mater. 24 (2012) 2459–2462.

[14] K. Zilberberg, S. Trost, H. Schmidt, T. Riedl, Solution processed vanadium pentoxide as charge extraction layer for organic solar cells, Adv. Energy Mater. 1 (2011) 377–381.

[15] Z. Tan, L. Li, C. Cui, Y. Ding, Q. Xu, S. Li, D. Qian, Y. Li, Solution-processed tungsten oxide as an effective anode buffer layer for high-performance polymer solar cells, J. Phys. Chem. C 116 (2012) 18626–18632.

[16] M.D. Irwin, J.D. Servaites, D.B. Buchholz, B.J. Leever, J. Liu, J.D. Emery, M. Zhang, J.H. Song, et al., Structural and electrical functionality of Nio interfacial films in bulk heterojunction organic solar cells, Chem. Mater. 23 (2011) 2218–2226.

[17] Y.Y. Cao, M.S. Denny, J.V. Caspar, W.E. Farneth, Q.J. Guo, A.S. Ionkin, et al., High-efficiency solution-processed Cu2ZnSn(S,Se)4 thin-film solar cells prepared from binary and ternary nanoparticles, J. Am. Chem. Soc. 134 (2012) 15644–15647.

[18] A. Carrete, A. Shavel, X. Fontane, J. Montserrat, J.D. Fan, M. Ibanez, E. Saucedo, A. Perez-Rodriguez, A. Cabot, Antimony-based ligand exchange to promote crystallization in spray-deposited Cu2ZnSnSe4 solar cells, J. Am. Chem. Soc. 135 (2013) 15982–15985.

[19] Z. Su, J.M.R. Tan, X. Li, X. Zeng, S.K. Batabyal, L.H. Wong, Cation substitution of solution-processed Cu_2ZnSnS_4 thin film solar cell with over 9% efficiency, Adv. Energy Mater. 5 (2015) 1500682.

[20] S. Ahmed, K.B. Reuter, O. Gunawan, L. Guo, L.T. Romankiw, H. Deligianni, A high efficiency electrodeposited Cu2ZnSnS4 solar cell, Adv. Energy Mater. 2 (2012) 253–259.

[21] F.J. Fan, B. Yu, Y.X. Wang, Y.L. Zhu, X.J. Liu, S.H. Yu, Z.F. Ren, Colloidal synthesis of Cu2CdSnSe4 nanocrystals and hot-pressing to enhance the Thermoelectric Figure-of-Merit, J. Am. Chem. Soc. 133 (2011) 15910–15913.

[22] M. Ibanez, R. Zamani, A. LaLonde, D. Cadavid, W.H. Li, A. Shavel, J. Arbiol, J.R. Morante, S. Gorsse, G.J. Snyder, A. Cabot, Cu2ZnGeSe4 nanocrystals: synthesis and thermoelectric properties, J. Am. Chem. Soc. 134 (2012) 4060–4063.

[23] G.K. Dalapati, S.K. Batabyal, S.M. -Panah, Z. Su, A. Kushwaha, T.I. Wong, H.F. Liu, T. Bhat, A. Iskandera, Y.-F. Lim, L.H. Wong, S. Tripathy, D. Chi, Sputter grown sub-micrometer thick Cu2ZnSnS4 thin film for photovoltaic device application, Mater. Lett. 160 (2015) 45–50.

[24] B.A. Schubert, B. Marsen, S. Cinque, T. Unold, R. Klenk, S. Schorr, H.W. Schock, Cu2ZnSnS4 thin film solar cells by fast coevaporation, Prog. Photovolt. 19 (2011) 93–96.

[25] W. Daranfed, M.S. Aida, N. Attaf, J. Bougdira, H. Rinnert, Cu2ZnSnS4 thin films deposition by ultrasonic spray pyrolysis, J. Alloy. Compd. 542 (2012) 22–27.

[26] K. Ramasamy, M.A. Malik, P. O'Brien, The chemical vapor deposition of Cu2ZnSnS4 thin films, Chem. Sci. 2 (2011) 1170–1172.

[27] T.K. Todorov, K.B. Reuter, D.B. Mitzi, High-efficiency solar cell with Earth-Abundant liquid-processed absorber, Adv. Mater. 22 (2010) 156.

[28] K. Tanaka, M. Oonuki, N. Moritake, H. Uchiki, Cu2ZnSnS4 thin film solar cells prepared by non-vacuum processing, Sol. Energy Mater. Sol. Cells 93 (2009) 583.

[29] C.P. Chan, H. Lam, C. Surya, Preparation of Cu2ZnSnS4 films by electrodeposition using ionic liquids, Sol. Energy Mater. Sol. Cells 94 (2010) 207.

[30] C. Meng, L. Li, W.Z. Fan, X.Y. Liu, Y. Sun, Y. Shen, Quaternary Cu2CdSnS4 nanoparticles synthesized by a simple solvothermal method, Chem. Phys. Lett. 534 (2012) 34–37.

[31] S.D. Sartale, B.R. Sankapal, M.L. Steiner, A. Ennaoui, Preparation of nanocrystalline ZnS by a new chemical bath deposition route, Thin Solid Films 480–481 (2005) 168.

[32] L. Nie, S. Liu, Y. Chai, R. Yuan, Spray pyrolysis deposition and photoresponse of Cu2CdSnS4 thin films, J. Anal. Appl. Pyrolysis 112 (2015) 363–368.

[33] ⟨http://www.stion.com/wp-content/uploads/2015/05/900-053-000-Rev-I_Stion-Limited-Warranty-For-PV-Modules.pdf⟩; downloaded from Stion.com on 4th November 2016.

[34] A. Karpinski, S. Berson, H. Terrissse, M. Mancini-Le Granvalet, S. Guillerez, L. Brohan, M. Richard-Plouet, Anatase colloidal solutions suitable for inkjet printing: enhancing lifetime of hybrid organic solar cells, Sol. Energy Mater. Sol. Cells 116 (2013) 27–33.